Regionalization of browning revealed by whole subcutaneous adipose tissue imaging

Corinne Barreau, Elodie Labit, Christophe Guissard, Jacques Rouquette, Marie-Laure Boizeau, Souleymane Gani Koumassi, Audrey Carrière, Yannick Jeanson, Sandra Berger-Müller, Cécile Dromard, et al.

Regionalization of Browning Revealed by Whole Subcutaneous Adipose Tissue Imaging

Corinne Barreau[1†], Elodie Labit[1†], Christophe Guissard[1], Jacques Rouquette[2], Marie-Laure Boizeau[2], Souleymane Gani Koumassi[2], Audrey Carrière[1], Yannick Jeanson[1], Sandra Berger-Müller[1], Cécile Dromard[1], Franck Plouraboué[3], Louis Casteilla[1] and Anne Lorsignol[1]**

Objective: White and brown adipose tissues play a major role in the regulation of metabolic functions. With the explosion of obesity and metabolic disorders, the interest in adipocyte biology is growing constantly. While several studies have demonstrated functional differences between adipose fat pads, especially in their involvement in metabolic diseases, there are no data available on possible heterogeneity within an adipose depot.

Methods: This study investigated the three-dimensional (3-D) organization of the inguinal fat pad in adult mice by combining adipose tissue clearing and autofluorescence signal acquisition by confocal microscopy. In addition, the study analyzed the expression of genes involved in adipocyte biology and browning at the mARN and protein levels in distinct areas of the inguinal adipose tissue, in control conditions and after cold exposure.

Results: Semiautomated 3-D image analysis revealed an organization of the fat depot showing two regions: the core was structured into segmented lobules, whereas the periphery appeared unsegmented. Perilipin immunostaining showed that most of the adipocytes located in the core region had smaller lipid droplets, suggesting a brown-like phenotype. qPCR analysis showed a higher expression of the browning markers *Ucp1*, *Prdm16*, *Ppargc1a*, and *Cidea* in the core region than at the periphery. Finally, cold exposure induced upregulation of thermogenic gene expression associated with an increase of UCP1 protein, specifically in the core region of the inguinal fat depot.

Conclusions: Altogether, these data demonstrate a structural and functional heterogeneity of the inguinal fat pad, with an anatomically restricted browning process in the core area.

Introduction

With the increase in the prevalence of obesity and metabolic disorders, the interest of scientists in white adipose tissue (WAT) is growing constantly. Since its principal function is to store and release lipids in response to energy-balance needs, understanding its biology appears crucial (1,2). WAT is located in distinct anatomical sites and exhibits a captivating plasticity at the tissue and/or cellular level. In addition to white adipocytes that contain a large unilocular vacuole, WAT also contains some multilocular adipocytes that are immunoreactive for the specific marker of brown adipocytes, uncoupling protein1 (UCP1) (3,4). This mitochondrial protein uncouples the functioning of the respiratory chain from ATP synthase, thus generating heat. The number of UCP1-positive adipocytes within WAT increases strongly when animals are exposed to cold or under adrenergic stimulation, through the "browning process" (3-6). These adipocytes are different from the "classical" brown adipocytes located in brown adipose tissue (BAT) (such as the interscapular depot in mice) in terms of origin, activation, and metabolism and are named "brown-like adipocytes," "beige," or "brite" (brown in white) adipocytes. The demonstration that UCP1-positive adipocytes could be easily detected in adult humans has strongly renewed the interest in BAT and the browning process (7,8).

[1] Stromalab, Universite´ de Toulouse, CNRS, EFS, INSERM, UPS, Toulouse, France. Correspondence: Louis Casteilla (louis.casteilla@inserm.fr) or Anne Lorsignol (anne.lorsignol@inserm.fr) [2] Institut des Techniques Avanc´ees du Vivant, Universite´ de Toulouse, CNRS, UPS, Toulouse, France [3] Institut de M´ecanique des Fluides, Universit´e de Toulouse, INPT, UPS, Toulouse, France.

†Corinne Barreau and Elodie Labit contributed equally to this work.

Funding agencies: This work was supported by the EU FP7 project DIABAT (Health-F2-2011-278373), a grant from the CNRS (PEPS MATH), and a grant from the Midi-Pyr´en´ees Region (DESR/12052900 and DESR/14050455).

The molecular pathways driving brown and white adipocyte differentiation or adipocyte hyperplasia and hypertrophy have now been well investigated and described (2,9). While a large number of studies have demonstrated that adipose depots differ from each other in terms of "adipocyte biology" (10), there is no investigation on putative heterogeneity within a fat depot, although different histology studies clearly have suggested that the emergence of brite adipocytes is heterogeneous inside a given fat pad (4,11,12). Since Wassermann's work in 1960 (13), very few data have become available on the global organization of adipose tissue. These investigations revealed that, in human embryo, WAT is made up of lobules corresponding to clusters of adipocytes, separated from each other by a structured extracellular matrix (ECM). In the liver, lobules make functional units essential to the functions of this organ (14). Depending on their location within a lobule, hepatocytes have different gene expression patterns inducing different metabolic functions, which is also known as "metabolic zonation" (15,16). Several studies have suggested that there is also heterogeneity among hepatic lobules (17,18). By analogy, the adipose tissue organization into lobules must be a fundamental element of adipose tissue homeostasis as it is present throughout adult life, in different species (19,20). Nevertheless, even though occasionally mentioned in the literature, the lobule level has not been fully investigated, leaving open several questions related to the organization, the functional heterogeneity, and the role of these adipose "units."

To investigate a putative heterogeneity in browning ability, we investigated the global organization of the adipose depot using three-dimensional (3-D) imaging of the whole subcutaneous inguinal adipose tissue of adult C57BL/6 mice. In order to facilitate light penetration, the fat pad was cleared by replacing the water-based intra-/extracellular fluid with a solution of high refractive index to match that of the cell membrane (21). Moreover, microstructural details can be revealed, without any treatment of the specimen by antibodies or dyes, by acquisition of the nonspecific autofluorescence signal (22). Using these technologies and semiautomated 3-D image analysis, we demonstrated here, for the first time, that subcutaneous adipose tissue displays strong structural heterogeneity. This fat pad can be subdivided into two regions: in the core, software processing identified segmented lobules with clusters of small adipocytes whereas, at the periphery, a nonsegmented region with bigger adipocytes was observed. This structural heterogeneity is associated with functional heterogeneity: we show that brite adipocytes are preferentially located inside lobules and that the browning process after cold exposure does not affect the whole tissue but preferentially takes place in the lobules.

Methods

Animals

All experiments were carried out in compliance with European Community Guidelines (2010/63/UE) and approved by the French ethics committee. Experiments were performed on 6- to 8-week-old male C57BL/6J mice (Harlan Laboratories). The mice were group-housed (3 or 4 per cage) in a temperature-controlled room (21°C or 4°C depending on experiments) on a 12 h light/dark cycle with free access to food and water. Cold exposure lasted 7 days.

Inguinal adipose tissue preparation

Mice were killed by cervical dislocation and inguinal fat pads were removed. Depending on experiments, adipose tissues were fixed in 4% paraformaldehyde solution for 24 hours at 4°C (immunostaining) or directly stored in RNA Later (Qiagen) until use (RNA extraction). For whole tissue 3-D imaging, fixed tissue was embedded in 1% agarose before being dehydrated by graded series of ethanol incubations and then cleared by incubation in benzyl alcohol-benzyl benzoate solution (BABB, 1:2 vol:vol ratio) (Sigma Aldrich). BABB treatment is used to facilitate visible light penetration through the specimens by replacing the water-based intra-/extracellular fluids with a solution of high refractive index to match that of the cell membrane. BABB thus induces light scattering between the cell membrane and the surrounding media thereby rendering the tissue specimens transparent to visible light (23). For 2-D imaging and immunohistochemistry, the fixed inguinal fat pads were cut into 300 µm serial horizontal sections with a vibratome (Campden).

In vivo, the inguinal adipose tissue is inserted into the back of the animal by its apex and the ventral insertion is located toward the groin (Figure 1A). For further studies, the inguinal adipose tissue was systematically oriented as shown in Figure 1B: the *X* axis was defined by the length of tissue with the apex at the left and the groin at the right. The *Y* orientation corresponded to the width of the tissue according to the animal's antero-posterior axis. The *Z* orientation corresponded to the thickness of the tissue defined by the "skin-to-muscle" axis.

Epifluorescence macroscopy: 2-D imaging of adipose tissue sections

Sections of 300 µm thickness were analyzed using autofluorescence signal without any previous staining. Image acquisition was performed using a MacroFluo Z16 APO macroscope (Leica). The objective used for observation and acquisition was a Planapo 2.0X WD 39 mm with a physical zoom (1.6). Samples were excited with a metal halide bulb (HXP, Osram) and a fluorescence excitation filter (HQ470/40). The emitted light was acquired through a band-pass filter HQ525/50 (Chroma Technology Corp.) by a CoolSNAP ES2 CCD camera (Roper) driven by the MetaVue software (Universal Imaging). Images were processed using Fiji software (NIH).

2-D image analysis was performed manually by identifying and drawing septa between adipocyte clusters. A lobule was defined as a surface closed by continuous septa. Quantification was carried out on the horizontal and median section of the inguinal fat pad. This analysis was done twice by the same person in a blinded way. The mean area occupied by identifiable lobules, after two blinded analysis on a representative sample, was 26.34 ± 0.62 mm^2.

Confocal microscopy: 3-D imaging of whole cleared fat pad

The autofluorescence signal of the whole cleared inguinal fat pad was acquired using a Confocal Laser Scanning microscope (LSM510 NLO, Carl Zeiss) with an EC-Plan-Neofluar 10×/0.3 objective, after excitation using a 488 nm argon laser. The whole tissue autofluorescence signal was collected with a 500–530 nm bandpass filter. Multiple positions were acquired with an overlap of 10% and a z-stack was performed. Final images were obtained by stitching all the acquired positions using image metadata Grid/collection stitching plugins of Fiji software (24).

The whole fat pad was characterized into segmentable (SLA) and nonsegmentable lobule areas (NSLA) and the lymph node and main vessels were removed from the picture using a semiautomated

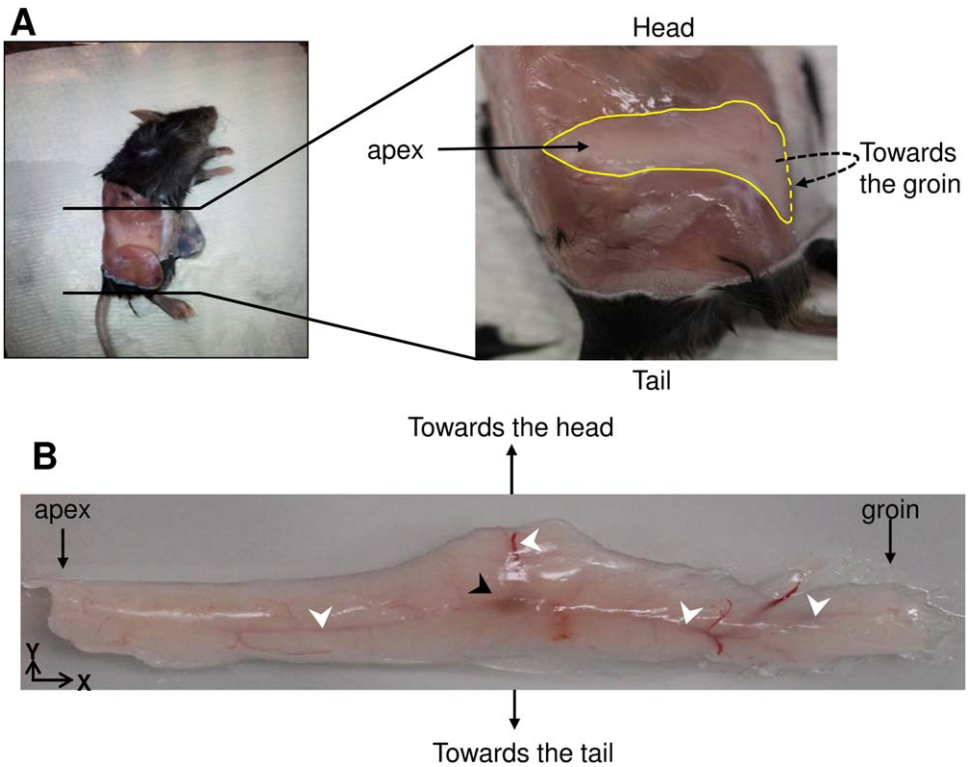

Figure 1 Anatomy of the right inguinal adipose tissue. (**A**) *In situ* orientation of the fat pad when the mouse is lying on its left side. (**B**) *Ex vivo* orientation for manipulation and imaging. The right adipose tissue is laid down on the muscle surface. The lymph node (black arrowhead) and main vascularization (white arrowheads) are visible by transparency.

method with the "surpass" module of Imaris software (Bitplane). The different volumes were extracted using the Imaris statistics module (Bitplane). A flow chart (Supporting Information, Figure S1) illustrating the successive steps of image analysis is given in the Supporting Information.

Immunohistochemistry

Adipose tissue sections of 300 μm thickness were incubated in blocking solution (2% Normal Horse Serum and 0.2% triton X-100 in PBS) at room temperature (RT) and incubated for 24 h at RT with primary antibody against perilipin (1:250, Sigma Aldrich) or UCP1 (1:5000, kindly provided by D. Ricquier). Sections were incubated overnight at 4°C with an Alexa 488-conjugated secondary antibody (Life Technology). Nuclei were stained with DAPI (Sigma Aldrich) and sections were mounted on a coverslip. Imaging was performed using a confocal Laser Scanning microscope (LSM510 NLO, Carl Zeiss). Morphometric analysis of lipid droplets was performed using Fiji software (NIH) on the horizontal and median section of the inguinal fat pad.

RNA extraction and quantitative real-time RT-PCR

Inguinal fat pads were placed on ice-cooled microscope slides and small blocks of SLA and NSLA were dissected using a scalpel and sharp forceps under a binocular loupe. Total RNA was isolated from SLA and NSLA samples of inguinal fat pad using Qiagen RNeasy kit (Qiagen) and purified using RNeasy microcolumns. RNA integrity and quantity were checked with Experion RNA StdSens Analysis Kit (Bio-Rad). Seven hundred and fifty nanograms of total RNA were reverse-transcribed using the High Capacity cDNA Reverse Transcription kit (Life Technologies/Applied Biosystem), SYBR Green PCR Master Mix (Life Technologies/Applied Biosystem), and 0.2 μM primers, on a Viia7^{TM}(Applied Biosystem) instrument. Relative gene expression was determined using the $2^{-\Delta\Delta CT}$ method and normalized to *36B4* level. Primers are listed in Table 1. All mRNA expression analysis was performed blind.

Statistical analysis

All data are expressed as means ± SEM. An unpaired *t* test was used to calculate final *P* values using GraphPad Prism software. Differences among groups were considered significant at $P < 0.05$.

Results

2-D imaging of inguinal fat pad reveals tissue heterogeneity

A general and representative view of the largest horizontal section of the fat pad is shown in Figure 2A. It corresponds to the section where the lymph node (LN) was the largest. Two regions could be distinguished in the adipose parenchyma: one in the core of the tissue where lobules were easily distinguished (Figure 2B) and a more diffuse region at the periphery where, although some septa were visible, closed, contiguous lobules could not be defined (Figure 2C).

TABLE 1 List and sequence of primers

	Forward primer	Reverse primer
Pparγ	AGTGTGAATTACAGCAAATCTCTGTTTT	GCACCATGCTCTGGTCAA
Pparα	GCAAGGCCTCAGGGGTAGCA	GCCGAATAGTTCGCG
36b4	AGTCGGAGGAATCAGATGAGGAT	GGCTGACTTGGTTGCTTTGG
Ap2	GATGCTTTGTGGGAACCTG	GCCATGCCTGCCACTTTC
Leptin	AAGACGATTGTCACCAGGATCAA	ACCCTCTGCTTGGCGGATA
Ucp1	AAGCTTGCTGTCACTCCTCTAC	TCTAGAGTCTGAGGAAAGGG
Ppargc1a	TGATGACAGTGAAGATCAAAGTGATAAAC	GGCGACACATCGAACATGAACAATGA
Cidea	CTAGCACCAAAGGCTGGTC	CACGCAGTTCCCACACACTC
Sdha	GTCCATACACCGAATAAGAGC	GTCCCCTGTGCTGGTATG
Cox7a1	CAGCGTCAGTCTGT	AGAAAACCGTGTGGCAGAGA
Cox8b	GAACCATGAAGCCAACGACT	GCGAAGTTCACAGTGGTTCC
Prdm16	GCACTTGCTTAAATACATATGACGTGTT	CAGCTGGAGGCCTTTCT
Mct1	GAGGTTCTCCAGTGCTGT	TCCATACATGTCATTGAGGCG
Mct4	AGTGCCATTGGTCTCGTG	CATACTTGTAACTTTGGTTGC

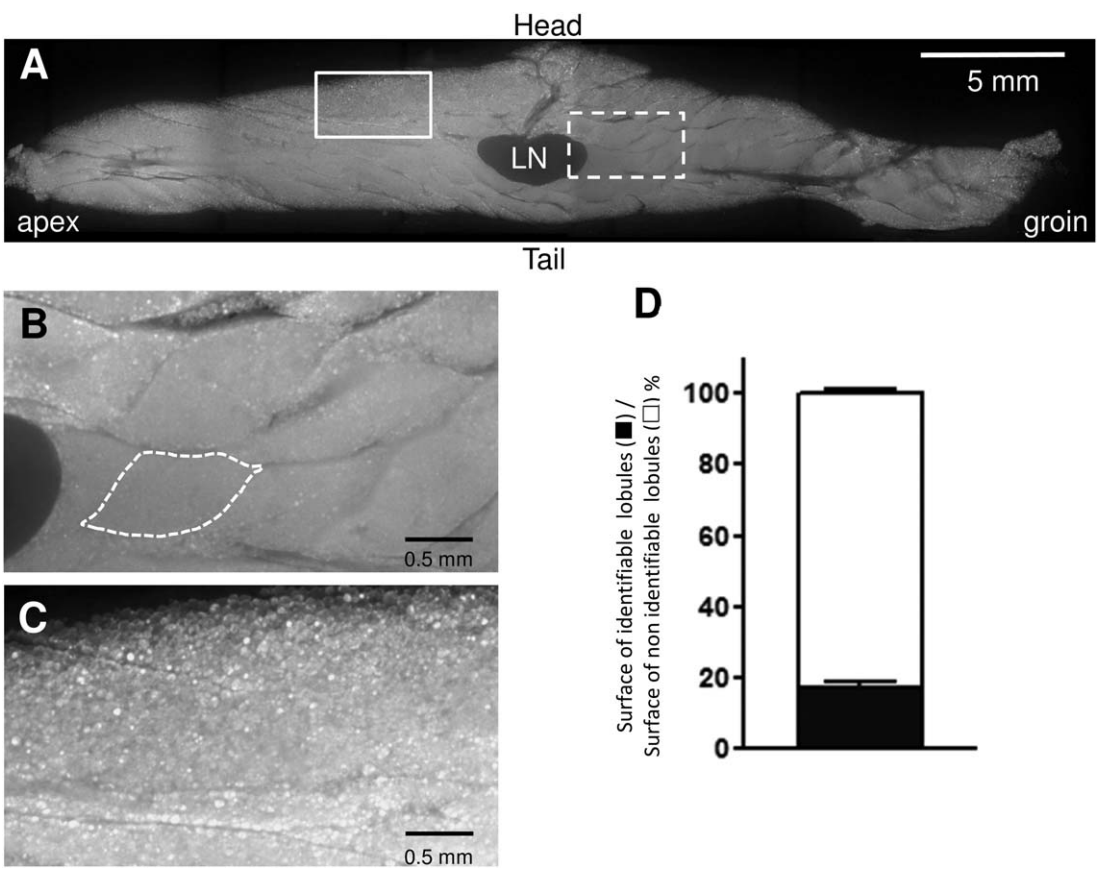

Figure 2 2-D imaging reveals structural heterogeneity of inguinal adipose tissue. (**A**) Image obtained with a microscope from a whole horizontal and median 300 μm section. Note the lymph node (LN) in the center of the fat pad section. (**B**) Magnification of the dotted square of panel A. In this part of the tissue, lobules are easily identifiable. An example of a delimited lobule is shown by the dotted line. (**C**) Magnification of the white square of panel A. In this part of the tissue, lobules are not easily identifiable. (**D**) Quantification of the areas where lobules are identifiable and nonidentifiable ($n = 5$ animals).

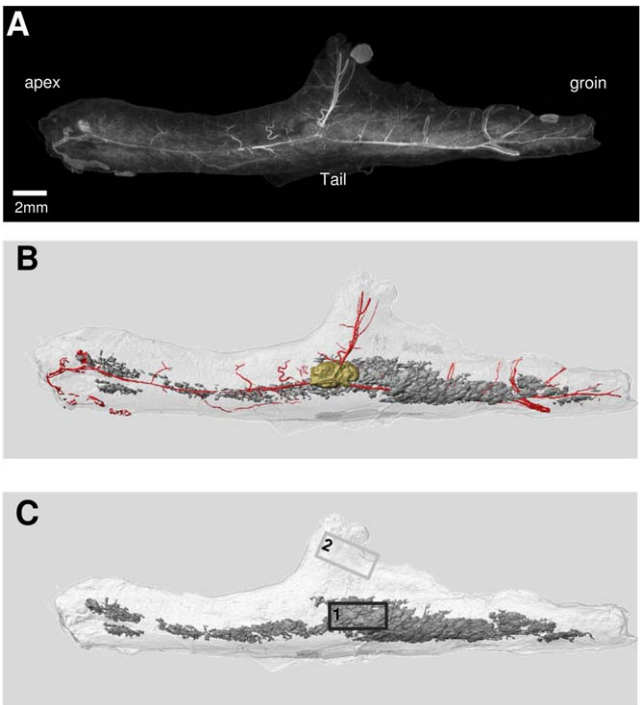

Figure 3 3-D confocal imaging of whole cleared inguinal adipose tissue confirms structural heterogeneity. (**A**) Image corresponding to the 3-D-visualization of inguinal fat depot after stitching process and before any image treatment. (**B**) Volume-rendering pseudoimage obtained after Imaris segmentation, illustrating lymph node (yellow) and main vascularization (red) of adipose tissue. These volumes were removed for further lobule segmentations. (**C**) Final pseudoimage showing two regions within inguinal fat pad: a central area with SLA (dark gray) and a surrounding area with NSLA (light gray). Rectangles 1 and 2 show regions in SLA and NSLA, respectively, in which further RT-PCR and immunostaining studies were performed (Figures 4 and 5).

Magnification of the images allowed each lobule to be manually delineated (Figure 2B, white-dotted line) and its surface area quantified. Fiji quantification revealed that the area occupied by identifiable lobules made up less than 20% of the surface of the median section (Figure 2D, $n = 5$ animals).

3-D imaging of whole cleared fat pad confirms a structural heterogeneity

To confirm the tissue heterogeneity revealed by the 2-D analysis, we performed 3-D imaging and semiautomated analysis of the whole cleared inguinal fat pad.

One 3-D-visualization of an inguinal fat depot after the stitching process and before any image treatment is shown in Figure 3A. Autofluorescence revealed anatomical details such as a high density of cells separated by ECM accumulation, lymph node, or main vascularization (Figure 3A and Supporting Information video). For further image analysis and to identify lobules as adipocyte clusters separated by ECM septa, the main blood vessels and lymph node (in red and yellow in Figure 3B) were removed from all z-images by Imaris software.

The semiautomated 3-D segmentation confirmed the tissue heterogeneity observed with 2-D images. The inguinal fat pad core was organized in segmentable lobules (Figure 3C, dark gray area), whereas the periphery was not structured in individualized lobules (Figure 3C, light gray area). These two regions are referred to as the "segmentable lobule area" (SLA) and the "nonsegmentable lobule area" (NSLA) in the following sections. The quantification of the SLA volume revealed that this part composed less than 10% of the total volume of the fat pad (SLA: 7.27 ± 2.8 mm^3 vs. NSLA: 75.73 ± 25.6 mm^3, $n = 3$ animals).

Brite adipocytes are preferentially localized within SLA

We next aimed to determine whether the above structural heterogeneity was associated with a functional heterogeneity. We investigated the morphology of mature adipocytes in both SLA and NSLA regions. Immunostaining of Perilipin, a specific protein surrounding the lipid droplets, revealed a smaller size of lipid droplets in the SLA than in the NSLA regions (Figure 4A and 4B Top) (400 ± 5.6 μm^2 compared to 1000 ± 310 μm^2 for SLA and NSLA, respectively, $P < 0.05$, $n = 5$ animals). Similar results were obtained when the distribution of lipid droplet sizes was investigated in the two regions: in SLA, adipocytes contained more small droplets (below 1000 μm^2) and fewer big droplets (>1000 μm^2) than the NSLA adipocytes (Figure 4B bottom).

This difference in lipid droplet size between SLA and NSLA led us to investigate whether adipocytes localized within these two different regions displayed the same biological features. Comparative analysis of gene expression of microdissected pieces of SLA and NSLA regions revealed different mRNA levels for genes corresponding to the brown oxidative adipocyte profile. *Ucp1* expression was dramatically increased in SLA compared to NSLA regions. This increase was associated with a higher expression of additional key thermogenic genes as well as mitochondrial markers (Figure 4C, $n = 15$ animals). Interestingly, the expression of monocarboxylate transporters *Mct1* and *Mct4*, which we have recently demonstrated to be involved in the browning process (26), was also significantly higher and lower in SLA compared to NSLA respectively. While no difference was detected in the content of mRNA coding for *Pparγ*, *aP2*, a lower expression of *Leptin* was observed in SLA (Figure 4C, $n = 15$ animals).

Cold exposure induces the apparition of brite adipocytes in the SLA region only

It is well known that chronic cold exposure largely increases the number of brite adipocytes in the subcutaneous white fat pad. We thus investigated the partitioning between SLA and NSLA and the expression of "browning" genes in the two regions after mice had been exposed to 4°C for 7 days.

Quantification of SLA and NSLA volumes using 3-D images of cleared inguinal fat pads revealed no statistical difference between control (21°C) and cold-exposed mice (Figure 5A, $n = 3$ animals). Strikingly, while no change was observed in NSLA after cold exposure (Figure 5B right panel, $n = 6$ animals), the data revealed an overexpression of *Pparα*, *Ppargc1a*, *Ucp1*, and *Mct1* genes in SLA (Figure 5B left panel, $n = 6$ animals) suggesting that the browning process occurred in SLA only. To confirm these data, immunostaining was performed to detect the protein UCP1. Consistently with quantitative real-time PCR (RT-qPCR) results, UCP1 immunostaining was increased only in the SLA of cold-exposed mice and this

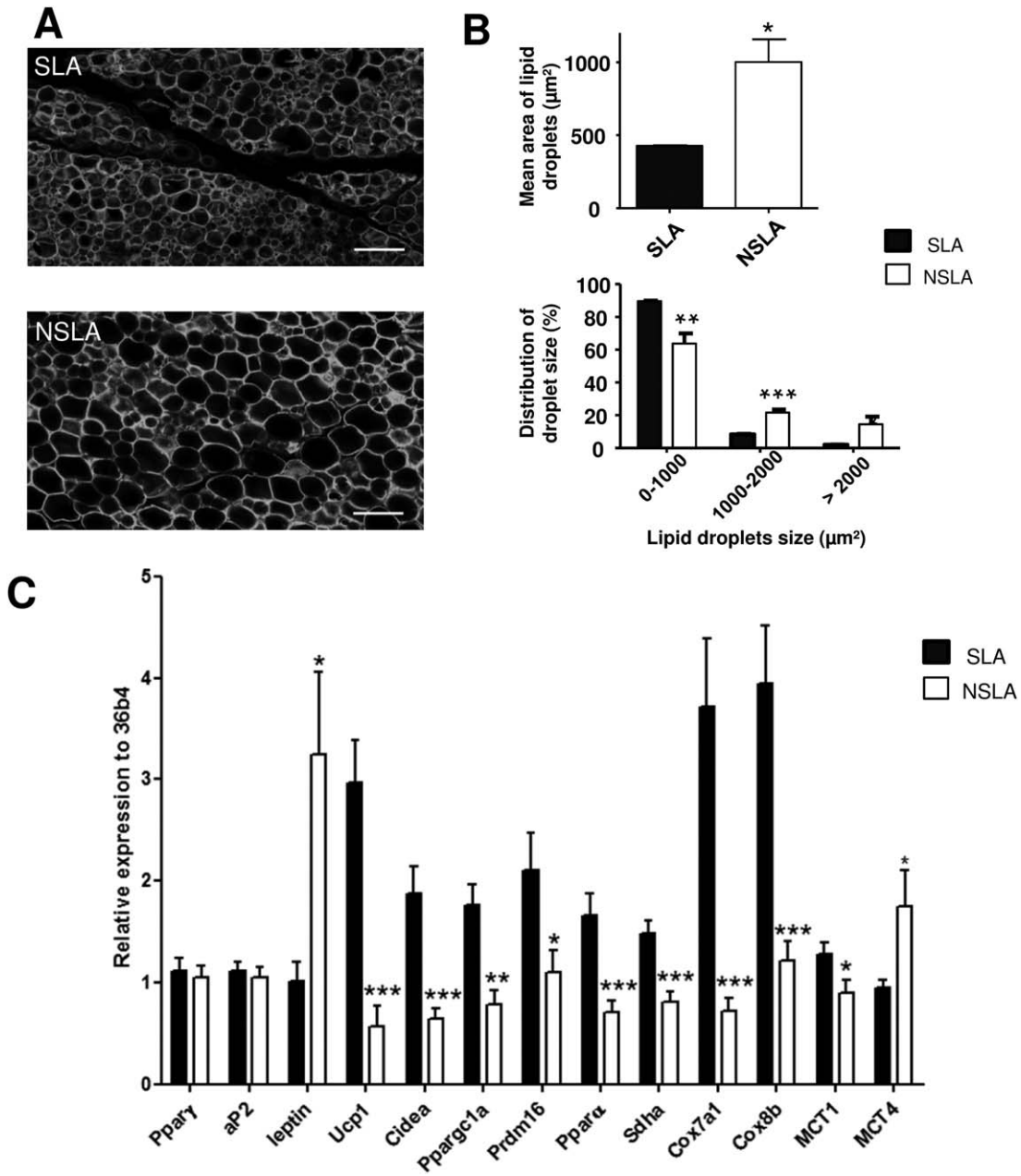

Figure 4 Cellular and molecular heterogeneity of inguinal fat pad. (**A**) Heterogeneity of lipid droplet sizes depending on the location within the tissue. Perilipin immunostaining in the SLA (top) and NLSA (bottom) (scale bar: 100 µm). (**B, top panel**) Quantification of mean size of lipid droplets depending on their location within the inguinal adipose tissue. (**B, bottom panel**) Distribution of lipid droplet sizes in SLA and NSLA (black and white bars, respectively) ($n = 5$ animals). (**C**) Heterogeneity of gene expression depending on the location within the tissue estimated by RT-qPCR in SLA and NSLA respectively ($n = 15$ animals). Values expressed as means ± SEM. $^{*}P<0.05$, $^{**}P<0.01$, $^{***}P<0.001$ SLA, vs. NSLA.

upregulation was mainly due to an increase in UCP1-positive cells (Figure 5C).

Altogether these data demonstrate that the structural heterogeneity revealed by our 3-D images of the whole inguinal fat pad reflects a cellular and molecular heterogeneity and that brite adipocytes were not scattered randomly through the whole adipose tissue but were preferentially located in SLA.

Discussion

While most studies demonstrate that subcutaneous and visceral fat depots are functionally different, without taking possible heterogeneity inside a fat depot into account, our study clearly shows that (i) inguinal adipose tissue is spatially organized and (ii) its structural regionalization is associated with a compartmentalization of browning ability.

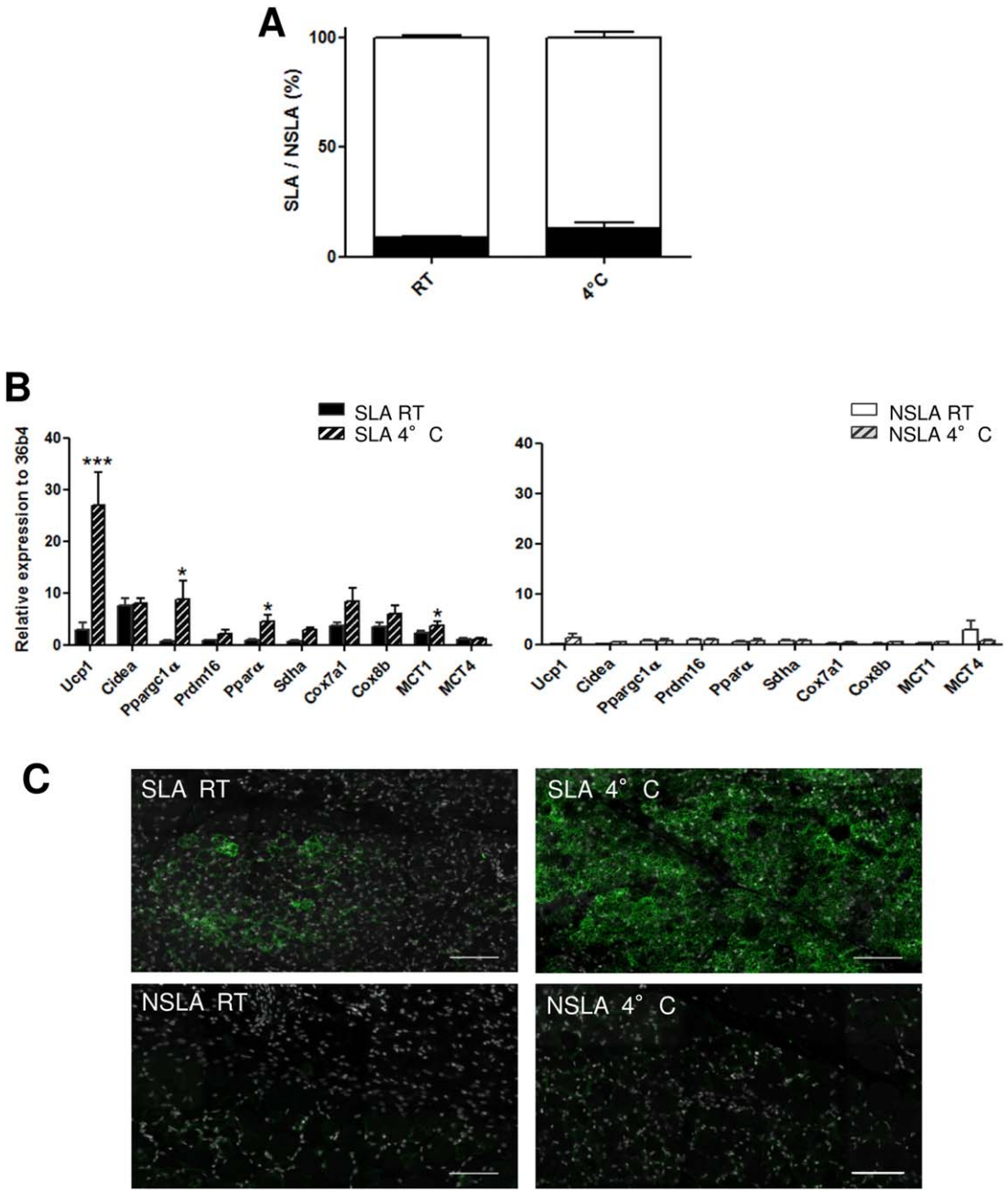

Figure 5 Cold-induced browning ability depends on the location in the tissue. (**A**) Quantification of the volume occupied by SLA and NSLA in mouse inguinal adipose tissue maintained at room temperature (RT) or at 4°C for 7 days. Analysis was carried out on 3-D images as described in Figure 3 ($n = 3$ animals). (**B**) The expression of genes involved in browning was estimated by RT-qPCR in SLA and NSLA of inguinal adipose tissue of mice exposed at RT or 4°C for 7 days ($n = 6$ animals). Values expressed as means ± SEM. $^{*}P < 0.05$, $^{***}P < 0.001$, SLA vs. NSLA. (**C**) Immunostaining of UCP1 protein in both areas of inguinal adipose tissue of mice maintained at RT or 4°C for 7 days. Nuclei were stained with DAPI (gray). Scale bar 100 μm.

An investigation of the organs anatomy is important for the understanding of physiological and pathological states. Under current conventional microscopy techniques, tissues and organs need to be sectioned but 3-D reconstructions of large samples are very laborious and difficult to obtain (22,23). The use of microscopy imaging applied to the entire mount is a reliable technical solution to such issues. Unfortunately, the scattering of imaging light due to the different refractive indices of the various structures limits optical imaging of thick tissues. Optical clearing of tissue by organic solvents, which make the biological tissue transparent by matching the refractory indexes of different tissue layers to those of the solvent, is becoming a prominent method for imaging thick tissue as it

overcomes these limitations (26). Adipose tissue has most often been sectioned to a thickness of less than 20–30 μm (27,28), which is smaller than the adipocyte diameter. Such investigations have made it difficult to draw relevant conclusions about the global organization of this tissue. This study reports the first use of optical clearing and confocal microscopy to investigate the global organization of the inguinal adipose depot. This strategy allowed us to image the whole inguinal adipose depot of adult mice.

In order to image microstructures at cell-size resolution, different cell populations are usually immunostained. However, the penetration of antibodies or dyes inside a thick tissue is always limited. To avoid this technical problem, imaging the signals emitted by endogenous fluorophores is an alternative to standard histological preparations for rapid examination of fresh biopsies and has been developed mainly in pathological diagnosis (22,29,30). As observed in other tissues (26,31), the intrinsic fluorescence of the inguinal adipose depot clearly showed microanatomical details such as lymph node, main vascularization, and septa between adipocyte clusters (Figure 3A and supplementary video). Intrinsic fluorescence is a composite signal that is difficult to analyze finely and that includes various putative molecules, located within different cell compartments (NADPH, lipo-pigments, flavin coenzymes, and so forth) (32,33). Although we have not pinpointed the exact source of tissue autofluorescence, this opens up new ways of imaging adipose tissue in 3-D in the future, including in humans.

We used a semiautomated computational approach to delineate 3-D volumetric adipose lobules, which were then turned into 3-D surface-rendered data. This approach enabled several samples to be compared. Although this approach is not completely automated and thus depends on the experimenter during image analysis, it is important to note that similar percentages of segmented and nonsegmented lobule areas were obtained with 2-D and 3-D images.

Whatever the imaging processes, the structural analysis clearly revealed two distinct regions: a core region with well identified segmented lobules and a peripheral region where segmentation was not possible (SLA and NSLA respectively). The most structured region, that is, SLA, only formed about 10%–20% of the whole tissue in our experimental conditions. This conclusion may be surprising as, in Wasserman's study, human embryonic and postembryonic adipose tissue is considered as entirely composed of lobules (13). This discrepancy between the earlier study and our result may reflect species and developmental differences. Moreover, other studies that described the presence of lobules in adipose tissue investigated neither their distribution nor their proportion within the whole fat pad (19,34). Preliminary investigations on other adipose depots in the mouse (including epididymal, mesenteric, and interscapular fat pads) suggest that a similar structural heterogeneity could be observed in some pads (data not shown). These results raise the question of the role and developmental origin of the two parts.

Our analysis reveals that lipid droplets were larger in the periphery than in the core region of the depot. This is consistent with higher expression of leptin in the NSLA region. In contrast, the smaller lipid droplets observed in the SLA were associated with the presence of UCP1-immunopositive adipocytes and a high expression level of browning genes. This presence of a significant number of brite adipocytes was not surprising since experiments were performed on animals maintained at 21°C, which is below the temperature of thermoneutrality in mice. This could be linked with a weak sympathetic nervous system activation that would explain the presence of such brite adipocytes.

After 7 days at 4°C, the ratio between SLA and NSLA volume had not changed. Consistently with previous reports (4,12), the number of UCP1-immunopositive adipocytes increased, but only in the SLA part. Further studies to investigate WAT browning process and brite adipocyte biology must consider this tissue compartmentalization when taking tissue samples. The relatively small volume dedicated to browning (10%–20% of the inguinal fat pad volume) raises questions about the physiological consequences of this tissue. It is noteworthy that brown adipocytes are highly thermogenic cells. After cold exposure, the activation of only 150–200 g of BAT in an adult human significantly contributes to the 80% increase in total energy expenditure (35). Our result definitively demonstrates not only that the structural heterogeneity of adipose tissue is associated with functional differences but also that the browning process is spatially restricted to a central part of the pad where lobules can be individualized. This opens up the question of the physiological relevance of this association. It is noteworthy that lobules are located near the main vasculature of the tissue. The colocation of brite adipocytes and lobules would be consistent with the specific link between brown adipocytes and vascularization required to import oxygen and nutrients and to export heat (36,37). Since the sympathetic nervous system is intimately involved in the browning process (4), it is also reasonable to speculate that the SLA is highly innervated, although no data concerning the fine organization of sympathetic innervation within the inguinal fat pad is available.

Taken together, our results, which demonstrate the specific location of browning associated with a structural heterogeneity of the inguinal adipose tissue, revive the debate on tissue organization, the developmental origins of the adipocyte lineage, and the plasticity between WAT and BAT. It emphasizes the fact that the anatomical and structural organization of adipose tissue needs to be revisited in all species and particularly in humans.

Acknowledgments

The authors are grateful to the Institut des Techniques Avancées du Vivant (ITAV, USR3505) and to the I2MC/UMR1048, Genome and Transcriptome Platform of Toulouse "Génopole."

References

1. Sethi JK, Vidal-Puig AJ. Thematic review series: Adipocyte biology. Adipose tissue function and plasticity orchestrate nutritional adaptation. *J Lipid Res* 2007;48:1253-1262.
2. Rosen ED, Spiegelman BM. What we talk about when we talk about fat. *Cell* 2014; 156:20-44.
3. Loncar D. Convertible adipose tissue in mice. *Cell Tissue Res* 1991;266:149-161.
4. Cousin B, Cinti S, Morroni M, et al. Occurrence of brown adipocytes in rat white adipose tissue: Molecular and morphological characterization. *J Cell Sci* 1992;103: 931-942.
5. Klingenspor M. Cold-induced recruitment of brown adipose tissue thermogenesis. *Exp Physiol* 2003;88:141-148.
6. Young P, Arch JR, Ashwell M. Brown adipose tissue in the parametrial fat pad of the mouse. *FEBS Lett* 1984;167:10-14.
7. Cereijo R, Giralt M, Villarroya F. Thermogenic brown and beige/brite adipogenesis in humans. *Ann Med* 2015;47:167-177.

8. Cannon B, Nedergaard J. Metabolic consequences of the presence or absence of the thermogenic capacity of brown adipose tissue in mice (and probably in humans). *Int J Obes* 2010;34:S7-16.
9. Peirce V, Carobbio S, Vidal-Puig A. The different shades of fat. *Nature* 2014;510: 76-83.
10. Tchkonia T, Thomou T, Zhu Y, et al. Mechanisms and metabolic implications of regional differences among fat depots. *Cell Metab* 2013;17:644-656.
11. Vitali A, Murano I, Zingaretti MC, Frontini A, Ricquier D, Cinti S. The adipose organ of obesity-prone C57BL/6J mice is composed of mixed white and brown adipocytes. *J Lipid Res* 2012;53:619-629.
12. Barbatelli G, Murano I, Madsen L, et al. The emergence of cold-induced brown adipocytes in mouse white fat depots is determined predominantly by white to brown adipocyte transdifferentiation. *Am J Physiol Endocrinol Metab* 2010;298: 53.
13. Wassermann F. The development of adipose tissue. *Compr Physiol. 2011, Supplement 15: Handbook of Physiology* 1965, pp. 87-100. doi:10.1002/cphy.cp05011
14. Gebhardt R, Matz-Soja M. Liver zonation: Novel aspects of its regulation and its impact on homeostasis. *World J Gastroenterol* 2014;20:8491-8504.
15. Jungermann K, Kietzmann T. Oxygen: Modulator of metabolic zonation and disease of the liver. *Hepatology (Baltimore, Md)* 2000;31:255-260.
16. Jungermann K, Kietzmann T. Zonation of parenchymal and nonparenchymal metabolism in liver. *Ann Rev Nutr* 1996;16:179-203.
17. Ishikawa T, Mori M, Ichikawa Y, Kitoh J, Yamashita K. Three-dimensional observations of spatial arrangement of hepatic zonation and vein system in mice and house musk shrews. *Anat Rec* 2000;260:228-237.
18. Teutsch HF. The modular microarchitecture of human liver. *Hepatology (Baltimore, Md)* 2005;42:317-325.
19. Hausman GJ, Kauffman RG. The histology of developing porcine adipose tissue. *J Anim Sci* 1986;63:642-658.
20. Macchi V, Tiengo C, Porzionato A, et al. Histotopographic study of the fibroadipose connective cheek system. *Cells Tissues Organs* 2010;191:47-56.
21. Ertürk A, Becker K, Jährling N, et al. Three-dimensional imaging of solvent-cleared organs using 3DISCO. *Nat Protoc* 2012;7:1983-1995.
22. Mori H, Borowsky AD, Bhat R, Ghajar CM, Seiki M, Bissell MJ. Laser scanning-based tissue autofluorescence/fluorescence imaging (LS-TAFI), a new technique for analysis of microanatomy in whole-mount tissues. *Am J Pathol* 2012;180:2249-2256.
23. Becker K, Jährling N, Saghafi S, Weiler R, Dodt H-UU. Chemical clearing and dehydration of GFP expressing mouse brains. *PloS One* 2012;7:
24. Preibisch S, Saalfeld S, Tomancak P. Globally optimal stitching of tiled 3D microscopic image acquisitions. *Bioinformatics* 2009;25:1463-1465.
25. Carriere A, Jeanson Y, Berger-Muller S, et al. Browning of white adipose cells by intermediate metabolites: An adaptive mechanism to alleviate redox pressure. *Diabetes* 2014;63:3253-3265.
26. Dodt HU, Leischner U, Schierloh A, et al. Ultramicroscopy: Three-dimensional visualization of neuronal networks in the whole mouse brain. *Nat Methods* 2007;4: 331-336.
27. Berry R, Church CD, Gericke MT, Jeffery E, Colman L, Rodeheffer MS. Imaging of adipose tissue. *Meth Enzymol* 2014;537:47-73.
28. Cinti S, Zingaretti MC, Cancello R, Ceresi E, Ferrara P. Morphologic techniques for the study of brown adipose tissue and white adipose tissue. *Methods Mol Biol* 2001;155:21-51.
29. Monici M. Cell and tissue autofluorescence research and diagnostic applications. *Biotechnol Ann Rev* 2005;11:227-256.
30. DaCosta RS, Andersson H, Cirocco M, Marcon NE, Wilson BC. Autofluorescence characterisation of isolated whole crypts and primary cultured human epithelial cells from normal, hyperplastic, and adenomatous colonic mucosa. *J Clin Pathol* 2005;58:766-774.
31. Brede C, Friedrich M, Jordan-Garrote AL, et al. Mapping immune processes in intact tissues at cellular resolution. *J Clin Investig* 2012;122:4439-4446.
32. Zipfel WR, Williams RM, Christie R, Nikitin AY, Hyman BT, Webb WW. Live tissue intrinsic emission microscopy using multiphoton-excited native fluorescence and second harmonic generation. *Proc Natl Acad Sci U S A* 2003;100:7075-7080.
33. Richards-Kortum R, Sevick-Muraca E. Quantitative optical spectroscopy for tissue diagnosis. *Ann Rev Phys Chem* 1996;47:555-606.
34. De Caro R, Aragona F, Herms A, Guidolin D, Brizzi E, Pagano F. Morphometric analysis of the fibroadipose tissue of the female pelvis. *J Urol* 1998;160:707-713.
35. Ouellet V, Labbé SMM, Blondin DP, et al. Brown adipose tissue oxidative metabolism contributes to energy expenditure during acute cold exposure in humans. *J Clin Investig* 2012;122:545-552.
36. Xue Y, Petrovic N, Cao R, et al. Hypoxia-independent angiogenesis in adipose tissues during cold acclimation. *Cell Metab* 2009;9:99-109.
37. Cao Y. Angiogenesis and vascular functions in modulation of obesity, adipose metabolism, and insulin sensitivity. *Cell Metab* 2013;18:478-489.